Characterizing Biphoton Spatial Wave Function Dynamics with Quantum Wavefront Sensing

Yi Zheng,[1,2] Zhao-Di Liu,[1,2,*] Rui-Heng Miao,[1,2,3] Jin-Ming Cui,[1,2,3] Mu Yang,[1,2] Xiao-Ye Xu,[1,2,3] Jin-Shi Xu,[1,2,3,†] Chuan-Feng Li,[1,2,3,‡] and Guang-Can Guo[1,2,3]

[1]*CAS Key Laboratory of Quantum Information, University of Science and Technology of China, Hefei 230026, China*
[2]*CAS Center for Excellence in Quantum Information and Quantum Physics, University of Science and Technology of China, Hefei 230026, China*
[3]*Hefei National Laboratory, University of Science and Technology of China, Hefei 230088, China*

(Received 20 January 2024; revised 27 March 2024; accepted 6 June 2024; published 16 July 2024)

With an extremely high dimensionality, the spatial degree of freedom of entangled photons is a key tool for quantum foundation and applied quantum techniques. To fully utilize the feature, the essential task is to experimentally characterize the multiphoton spatial wave function including the entangled amplitude and phase information at different evolutionary stages. However, there is no effective method to measure it. Quantum state tomography is costly, and quantum holography requires additional references. Here, we introduce quantum Shack-Hartmann wavefront sensing to perform efficient and reference-free measurement of the biphoton spatial wave function. The joint probability distribution of photon pairs at the back focal plane of a microlens array is measured and used for amplitude extraction and phase reconstruction. In the experiment, we observe that the biphoton amplitude correlation becomes weak while phase correlation shows up during free-space propagation. Our work is a crucial step in quantum physical and adaptive optics and paves the way for characterizing quantum optical fields with high-order correlations or topological patterns.

DOI: 10.1103/PhysRevLett.133.033602

Introduction.—The photon is a promising system in fundamental quantum physics and applied quantum techniques [1]. Its spatial degree of freedom is the core of high-dimensional quantum communication and quantum imaging [2], including ghost imaging [3], imaging with undetected photons [4], image distillation [5], and superresolution imaging [6,7]. Developing experimental methods to characterize the entangled multiphoton states is a basic task [8]. For the spatial state (sometimes called the wave function [9]), direct coincidence counting can reveal only the joint probability distribution (JPD), i.e., the squared modulus of the wave function [10], while effective phase measurement methods will become useful in various applications like information encoding [11], biomedical phase imaging [12], and aberration cancellation. Moreover, photons are prone to various evolution and modulation processes, so observing the state dynamics is even more exciting and challenging.

Researches on biphoton phase measurement can be inspired by classical methods. A prominent type is holography [13], which needs a reference beam for interference. It has the highest accuracy and is very suitable for characterizing transparent objects. In quantum optics, polarization entanglement enables phase-shifting holography [14–16], and biphoton interference has been employed to measure the biphoton spatial wave function [17]. However, the reference beam may contain aberrations and is not always available. Starting from Zernike's phase contrast microscopy [18], one type of reference-free method is selecting a part of the unknown field as the reference, including some weak measurement methods [9,19,20]. Our group used the setup devised by Kocsis *et al.* [21] to obtain the phase gradient distribution [22] for phase reconstruction [23,24] and named it the weak measurement wavefront sensor [25,26]. Like some shearing methods, it is an interference of the original beam with a slightly displaced one. Then, our group extended it to the multiphoton case [27], which requires JPD measurement of photons. However, weak measurement methods require a high signal-to-noise ratio, which is difficult for biphoton fields in experiments. There are other methods which do not need any reference. State tomography [28] requiring a huge number of projection bases is possible but impractical. Here, we consider the celebrated Shack-Hartmann wavefront sensing (SHWS) [29], which uses a microlens array to project the phase gradient at each aperture to the displacement of the focused spot [25,30]. Supplemental Material [31] introduces basic concepts of SHWS.

In this proof-of-principle work, we introduce and implement quantum SHWS (QSHWS) by measuring the JPD of photon pairs from spontaneous parametric down-conversion (SPDC) [32,33] at the focal plane of the microlens array. To our knowledge, this is the first single-measurement and reference-free biphoton phase

measurement method. As for the JPD measurement, traditional scanning and coincidence counting method [10] is time consuming. In 2018, Defienne *et al.* demonstrated that it can be calculated from multiple frames taken by an electron-multiplying charge-coupled device (EMCCD) or single-photon avalanche photodiode array camera [34–36], which we refer to as the multiple frame method. Then, we focus on the biphoton propagation dynamics as an example. Chan, Torres, and Eberly [37] derived that SPDC photon pairs would be less correlated in position after free-space propagation [38] while phase correlation shows up. We use QSHWS to measure the biphoton state after free-space propagation and show they agree with theoretical predictions using double-Gaussian approximation [33,37,39,40]. Furthermore, we use a spatial light modulator (SLM) to encode a hyperbolic paraboloid (saddle) phase pattern for detection. Finally, we describe potential applications of QSHWS in biphoton physical [41] and adaptive optics [42,43].

Theory.—We consider photon pairs with a definite polarization and wavelength. Denoting the spatial wave function as $\psi(\boldsymbol{\rho}_1,\boldsymbol{\rho}_2)$ and its phase $\phi(\boldsymbol{\rho}_1,\boldsymbol{\rho}_2) = \arg\psi(\boldsymbol{\rho}_1,\boldsymbol{\rho}_2)$, when the postselected position of photon 1 $\boldsymbol{\rho}_1$ takes all the values inside a microlens aperture S_1, the conditional state of photon 2 is generally mixed, described by the reduced density matrix $\hat{\varrho}_2 = \int_{S_1} d\boldsymbol{\rho}_1 \langle\boldsymbol{\rho}_1|\psi\rangle\langle\psi|\boldsymbol{\rho}_1\rangle$ and its function in the position basis $\varrho_2(\boldsymbol{\rho}_2',\boldsymbol{\rho}_2) = \langle\boldsymbol{\rho}_2'|\hat{\varrho}_2|\boldsymbol{\rho}_2\rangle = \int_{S_1} d\boldsymbol{\rho}_1 \psi(\boldsymbol{\rho}_1,\boldsymbol{\rho}_2')\psi^*(\boldsymbol{\rho}_1,\boldsymbol{\rho}_2)$ (corresponding to the mutual coherence function [25,44–46]). If a single-photon pure state is used, from the spot centroid displacement $\Delta\boldsymbol{\rho}$ from the center of another aperture S_2 at the camera, the phase gradient at S_2 is calculated by $(2\pi/\lambda)\sin[\arctan(\Delta\boldsymbol{\rho}/f_{\mathrm{SH}})]$, where f_{SH} is the microlens focal length. However, using the mixed state $\hat{\varrho}_2$, the measured phase gradient becomes [25,47] (see Supplemental Material [31] for a full derivation)

$$\frac{\int_{S_2} d\boldsymbol{\rho}_2 \mathrm{Im}\nabla_1\varrho_2(\boldsymbol{\rho}_2,\boldsymbol{\rho}_2)}{\int_{S_2} d\boldsymbol{\rho}_2\varrho_2(\boldsymbol{\rho}_2,\boldsymbol{\rho}_2)} = \frac{\int_{S_1} d\boldsymbol{\rho}_1 \int_{S_2} d\boldsymbol{\rho}_2 |\psi(\boldsymbol{\rho}_1,\boldsymbol{\rho}_2)|^2 \nabla_2\phi(\boldsymbol{\rho}_1,\boldsymbol{\rho}_2)}{\int_{S_1} d\boldsymbol{\rho}_1 \int_{S_2} d\boldsymbol{\rho}_2 |\psi(\boldsymbol{\rho}_1,\boldsymbol{\rho}_2)|^2}. \quad (1)$$

When the aperture is sufficiently small, S_1 and S_2 can be approximated by points $\boldsymbol{\rho}_1$ and $\boldsymbol{\rho}_2$, and Eq. (1) becomes the partial phase gradient $\boldsymbol{k}_2(\boldsymbol{\rho}_1,\boldsymbol{\rho}_2) = \nabla_2\phi(\boldsymbol{\rho}_1,\boldsymbol{\rho}_2)$. Exchanging $\boldsymbol{\rho}_1$ and $\boldsymbol{\rho}_2$ yields another partial gradient $\boldsymbol{k}_1(\boldsymbol{\rho}_1,\boldsymbol{\rho}_2) = \nabla_1\phi(\boldsymbol{\rho}_1,\boldsymbol{\rho}_2)$. The joint phase can be reconstructed by line integral [27]:

$$\phi(\boldsymbol{\rho}_1,\boldsymbol{\rho}_2) = \int_{(\mathbf{0},\mathbf{0})}^{(\boldsymbol{\rho}_1,\boldsymbol{\rho}_2)} \boldsymbol{k}_1(\boldsymbol{\rho}_1',\boldsymbol{\rho}_2')\cdot d\boldsymbol{\rho}_1' + \boldsymbol{k}_2(\boldsymbol{\rho}_1',\boldsymbol{\rho}_2')\cdot d\boldsymbol{\rho}_2'. \quad (2)$$

For the amplitude part, with the measured JPD $\Gamma_{\mathrm{SH}}(\boldsymbol{\rho}_1,\boldsymbol{\rho}_2)$ at the microlens focal plane, assuming each microlens is lossless and its incoming beam does not escape its aperture, the JPD of two apertures $\Gamma(\boldsymbol{\rho}_1,\boldsymbol{\rho}_2) \approx \int_{S_1} d\boldsymbol{\rho}_1' \int_{S_2} d\boldsymbol{\rho}_2' \Gamma_{\mathrm{SH}}(\boldsymbol{\rho}_1',\boldsymbol{\rho}_2')$ (here, S_1 and S_2 are centered by $\boldsymbol{\rho}_1$ and $\boldsymbol{\rho}_2$, respectively), which equals $\int_{S_1} d\boldsymbol{\rho}_1' \int_{S_2} d\boldsymbol{\rho}_2' |\psi(\boldsymbol{\rho}_1',\boldsymbol{\rho}_2')|^2$. The reconstructed wave function is, thus, $\sqrt{\Gamma(\boldsymbol{\rho}_1,\boldsymbol{\rho}_2)}\exp[i\phi(\boldsymbol{\rho}_1,\boldsymbol{\rho}_2)]$.

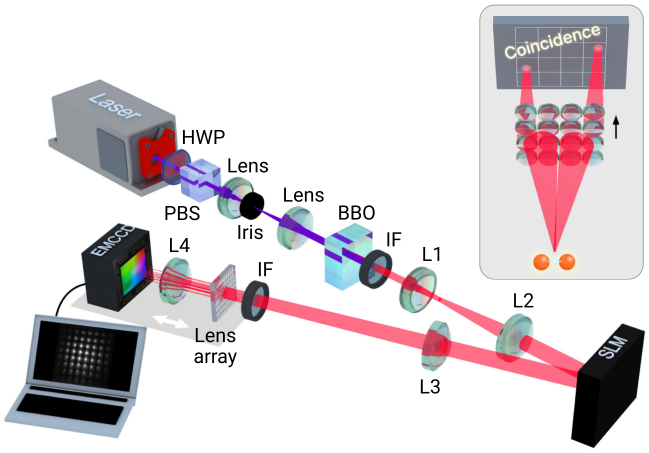

FIG. 1. The experimental setup. A 405-nm, horizontally polarized laser beam is shaped by two lenses and an iris. Then, it pumps a BBO crystal to produce collinear type-I SPDC photon pairs and is filtered out by a long-pass interference filter (IF). Two Fourier lenses (L1 and L2) project the photons from the BBO to the SLM. Then another Fourier lens (L3) projects the photons to the microlens array. A bandpass IF at (810 ± 5) nm selects degenerate SPDC photon pairs. An imaging lens (L4) images the photons from the focal plane of the microlens array to the EMCCD sensor. The microlens array, L4, and EMCCD can be displaced by a distance. The inset shows the basic idea of quantum Shack-Hartmann wavefront sensing.

If the two photons are indistinguishable $\psi(\boldsymbol{\rho}_1,\boldsymbol{\rho}_2) = \psi(\boldsymbol{\rho}_2,\boldsymbol{\rho}_1)$, only one phase gradient distribution can be measured. Without loss of generality, let it be $\boldsymbol{k}_1(\boldsymbol{\rho}_1,\boldsymbol{\rho}_2)$. Then, $\boldsymbol{k}_2(\boldsymbol{\rho}_1,\boldsymbol{\rho}_2) = \boldsymbol{k}_1(\boldsymbol{\rho}_2,\boldsymbol{\rho}_1)$, and the reconstructed $\phi(\boldsymbol{\rho}_1,\boldsymbol{\rho}_2)$ has exchange symmetry.

Experimental setup.—The experimental setup is shown in Fig. 1. A pump laser at 405 nm is incident on a β-barium borate (BBO) crystal. Degenerate near-collinear type-I SPDC photon pairs pass through two Fourier lenses, get reflected by a SLM, pass through another Fourier lens, and arrive at the microlens array. The width of each microlens is 0.3 mm. An imaging lens is inserted at the midpoint of the microlens array and the EMCCD sensor. See Supplemental Material [31] for details.

Data processing.—In one measurement, the EMCCD takes multiple frames, and a threshold determines whether pixels of each frame have at least one photon. In the multiple frame method, the JPD is calculated by the covariance of the counts at two pixels, which, however, suits only for biphoton states with narrow conditional probability distributions (CPDs, with the position of one

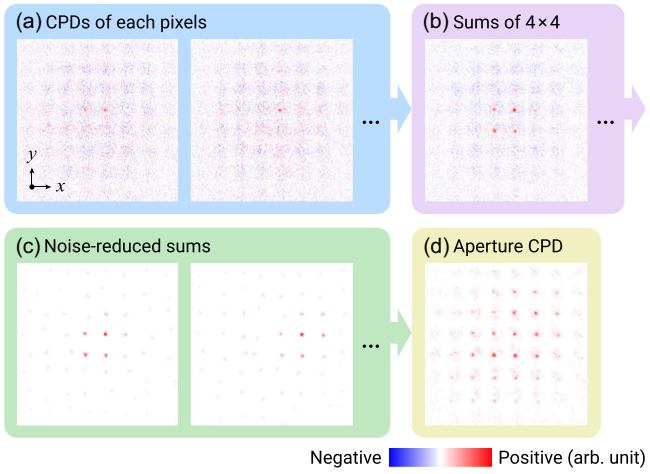

FIG. 2. Calculation of the aperture CPD. (a) The single-pixel CPDs from the multiple frame method. (b) The sum of 16 CPDs of a 4×4-pixel segment in (a). (c) Noise-reduced distributions from (b). (d) The sum of all the distributions in (c), which is the aperture CPD. The 7-cm propagation data are used as an example. See Supplemental Material [31] for more distribution graphs.

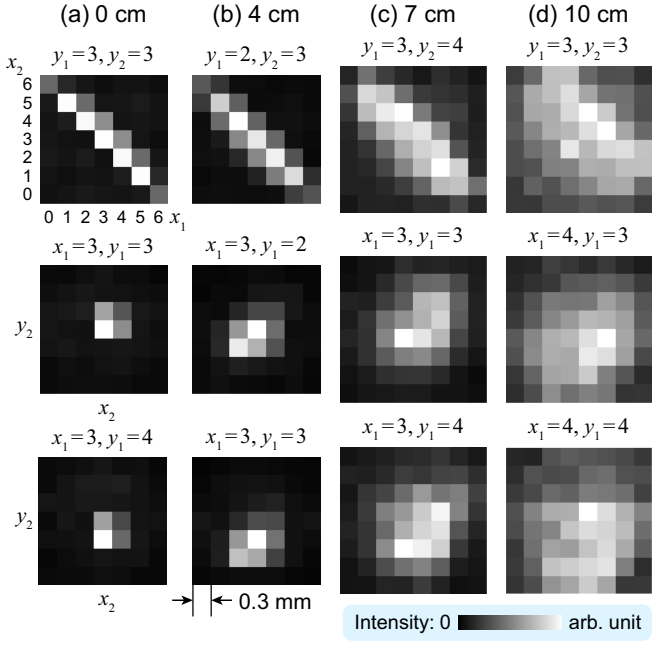

FIG. 3. Amplitude correlation and CPDs of SPDC photon pairs with (a) no propagation; (b) 4-cm propagation; (c) 7-cm; and (d) 10-cm. The first line is the x_1, x_2 distribution when the indices (starting from 0) of y_1, y_2 are given. The other two are CPDs of given apertures x_1, y_1.

photon given) due to its signal-to-noise ratio [35,38]. Also, photon intensity or sensor efficiency fluctuation results in a positive background in the calculated JPD, so a successive frame formula is mainly used in subsequent works [5,15,43], which will cause more noise in the JPD [7], and the background removal is not effective in our experiments. We develop a brightness separation formula where frames registering too many or few photons are discarded, and the background is basically eliminated.

Single-pixel CPDs of pixels within an aperture are summed to obtain the aperture CPD, but direct summation will distort the result. We choose to divide the aperture into several 4×4-pixel segments, sum CPDs over each segment first, and reduce the noise before being summed for the final aperture CPD. Figure 2 illustrates the processes. Finally, the centroid positions of the spots are calculated from the aperture CPD and converted to the phase gradient distribution.

An algorithm is required to realize the phase reconstruction in Eq. (2). For the four-dimensional phase distribution, the traditional zonal and modal methods [24] which require large matrix operations is difficult to implement. We adapt the method based on random point spreading and averaging in Ref. [27]. Supplemental Material [31] provides all details of data processing.

Biphoton propagation dynamics.—Using the microlens array, the biphoton position anticorrelation after three Fourier lenses with the SLM off can be observed easily, as shown in Fig. 3(a). The anticorrelation is not aperture to aperture, because its center is not a grid point of the microlens array.

However, the phase cannot be reconstructed without magnification for biphoton states with strong position correlation (see discussion below). To demonstrate the phase measurement, we need states with wider CPDs. Because of the immaturity of arbitrary two-photon interaction and modulation, more general correlated phase patterns cannot be generated experimentally. We choose to measure the correlated phase of propagated SPDC photon pairs. Before propagation, their wave function can be approximated by a double-Gaussian function (unnormalized) [33,37,39,40]:

$$\psi_{\mathrm{dG}}(\boldsymbol{\rho}_1, \boldsymbol{\rho}_2) = \exp\left(-\frac{|\boldsymbol{\rho}_1 + \boldsymbol{\rho}_2|^2}{4\sigma_+^2} - \frac{|\boldsymbol{\rho}_1 - \boldsymbol{\rho}_2|^2}{4\sigma_-^2}\right). \quad (3)$$

In the momentum space (angular spectrum [48]), it is the Fourier transform of Eq. (3):

$$\tilde{\psi}_{\mathrm{dG}}(\boldsymbol{q}_1, \boldsymbol{q}_2) = \exp\left(-\frac{\sigma_+^2|\boldsymbol{q}_1 + \boldsymbol{q}_2|^2}{4} - \frac{\sigma_-^2|\boldsymbol{q}_1 - \boldsymbol{q}_2|^2}{4}\right). \quad (4)$$

After propagating a distance z, a phase $\exp[-iz(|\boldsymbol{q}_1|^2 + |\boldsymbol{q}_2|^2)/(2k)]$ is added to the angular spectrum and, thus, $\sigma_\pm^2 \to \sigma_\pm^2 + iz/k$, where $k = 2\pi/\lambda$ and $\lambda = 810$ nm. Substituting the new complex $\sigma_\pm^2$ into Eq. (3) yields the new wave function with phase correlation. When $z = k\sigma_+\sigma_-$, the photons have no amplitude correlation, and entanglement exists only in the phase [37]. The amplitude correlation direction switches when $z > k\sigma_+\sigma_-$.

Previously, the biphoton JPD at intermediate distances cannot be measured using the multiple frame method [38]. Now, we reconstruct the wave functions of SPDC photon pairs propagating 4, 7, and 10 cm. Data of farther distances are still limited by the signal-to-noise ratio. The position correlation patterns and selected CPDs are shown in Figs. 3(b)–3(d), where the anticorrelation becomes weaker and CPDs become wider as z increases.

The theoretical phases of conditional wave functions are approximately spherical waves at twice the actual propagation distances, which can be explained in the next section. First, we do not interpolate the phase gradient distribution, and the reconstructed phase of conditional wave functions at a near-center aperture are fitted by phases of spherical waves at distances 8, 14, and 20 cm with displacements to be determined as shown in Fig. 4(a). The coefficients of determination (R^2) characterizing the similarity are also given, showing the reconstructed phases fit well with theory where the JPD values are higher (otherwise, the noise in the aperture CPDs distorts the phase gradient). As the phases of the wave functions are quadratic, their gradients are linear functions of the coordinates, valid for linear interpolation.

Then, we reconstruct wave functions from the interpolated (10 times) JPDs of two apertures and gradient distributions. Selected slices of them are shown in Fig. 4(b), where the theoretical counterparts from Eq. (3) are also plotted ($\sigma_+ \approx 13.43$ μm, $\sigma_- \approx 1.143$ mm; see Supplemental Material [31] for the calculation, which includes Ref. [49] about the refractive indices of BBO). Without interpolation, the phase patterns may be difficult to recognize from phase values modulo 2π. In the conditional wave functions, the center of the paraboloid phase pattern is anticorrelated with the given point. In regions where JPD values are higher, the reconstructed wave functions fit well with the theory. If these wave functions are Fourier transformed, the positive momentum correlation and the global paraboloid phase can be observed, as shown in Supplemental Material [31].

Note that a classically correlated photon pair has almost no momentum correlation, so measuring the JPD in the momentum space can tell whether they are entangled [10,50]. In Supplemental Material [31], we give a form of mixed two-photon state with position anticorrelation and briefly analyze its propagation and the measured values, compared with the entangled state above.

Phase modulation.—If a phase pattern $\Phi(\boldsymbol{\rho})$ is added on the SLM, the biphoton wave function at the SLM is multiplied by $\exp[i\Phi(\boldsymbol{\rho}_1) + i\Phi(\boldsymbol{\rho}_2)]$. Letting the Fourier transform of $\exp[i\Phi(\boldsymbol{\rho})]$ be $G(\boldsymbol{\rho}) = \int d\boldsymbol{\rho}' \exp[i\Phi(\boldsymbol{\rho}') - ik\boldsymbol{\rho}\cdot\boldsymbol{\rho}'/f_3]$, where f_3 is the focal length of the third Fourier lens, the wave function at the microlens array becomes $\psi(\boldsymbol{\rho}_1, \boldsymbol{\rho}_2) * [G(\boldsymbol{\rho}_1)G(\boldsymbol{\rho}_2)]$. Assuming the photon pairs are originally perfectly anticorrelated $\psi(\boldsymbol{\rho}_1, \boldsymbol{\rho}_2) = \exp(-|\boldsymbol{\rho}_1|^2/\sigma_-^2) \times \delta(\boldsymbol{\rho}_1 + \boldsymbol{\rho}_2)$, it is

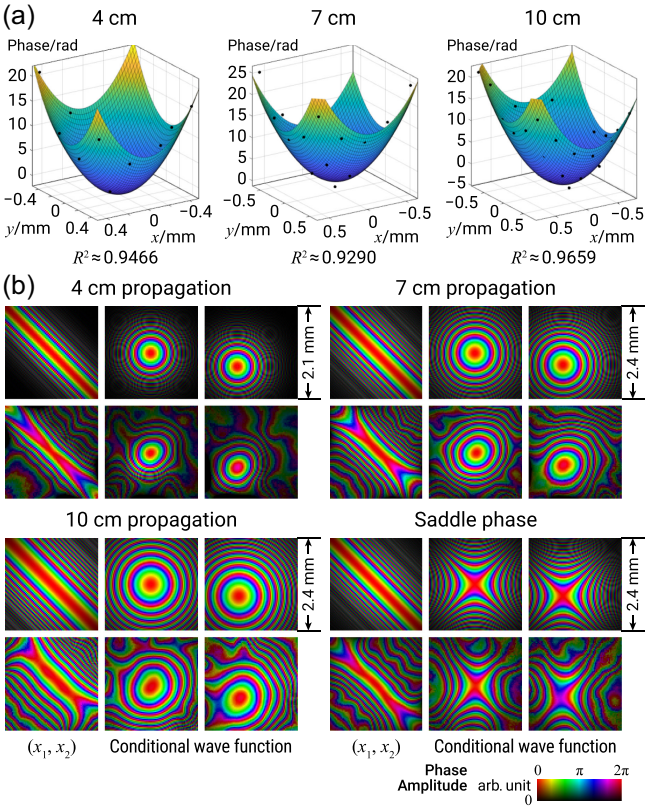

FIG. 4. (a) The reconstructed phase distributions of conditional wave functions without interpolation. The given points for the three conditional wave functions are indices (3,3), (4,4), and (4,3) respectively. Dots are the reconstruction results, and curves are theoretical phases with fitted displacement values. Dots away from zero are omitted, as their CPDs are smaller and vulnerable to errors. The R^2 values are given. (b) Theoretical double-Gaussian wave functions and experimentally reconstructed ones from interpolated phase gradients. For each biphoton state, the conditional wave function of x_1, x_2 with y_1, y_2 fixed at the center and two conditional wave functions of x_2, y_2 with two given (x_1, y_1) points (the first point is the center, and the second one is on the top right side, $0.3\sqrt{2}$ mm from the center) are shown. See Supplemental Material [31] for more conditional wave functions.

$$\left[G(\boldsymbol{\rho}_2)\exp\left(-\frac{|\boldsymbol{\rho}_1 - \boldsymbol{\rho}_2|^2}{\sigma_-^2}\right)\right] *^{(\boldsymbol{\rho}_2)} G(\boldsymbol{\rho}_1 + \boldsymbol{\rho}_2), \quad (5)$$

where the convolution performs only on $\boldsymbol{\rho}_2$ (see Supplemental Material [31] for its derivation). If $\sigma_- \to +\infty$ (the anticorrelated Einstein-Podolsky-Rosen state [51]), the conditional wave function with a given $\boldsymbol{\rho}_1$ is $G(\boldsymbol{\rho}_2) *^{(\boldsymbol{\rho}_2)} G(\boldsymbol{\rho}_1 + \boldsymbol{\rho}_2)$, which is the Fourier transform of $\exp[i2\Phi(\boldsymbol{\rho}_2)]$ displaced by $-\boldsymbol{\rho}_1$.

Adding a paraboloid phase $\Phi(\boldsymbol{\rho}) = -kz|\boldsymbol{\rho}|^2/(2f_3^2)$ on the SLM can simulate the propagation of z. The Fourier transform of $\exp[i2\Phi(\boldsymbol{\rho})]$ is a spherical wave at $2z$ in classical optics, and, thus, the conditional wave functions take this form. If a saddle phase $-a(x^2 - y^2)$ is added,

it propagates forward in the x direction and backward in y, resulting in the saddle phase in the conditional wave functions. We choose the forward and backward distance to be 7 cm. In the reconstructed phase as shown in Fig. 4(b), the magnitudes at the x and y directions are slightly different, which is possibly caused by a slight wavefront curvature of the pump beam, the obliquity of the SLM, or the deviation of the imaging lens magnification factor from -1. As the latter two can be eliminated, this method may be used to detect the low-order global phase of photon pairs correlated in position, which is hard to measure without propagation.

Discussion.—In this work, we introduced the quantum Shack-Hartmann wavefront sensing method to reconstruct the biphoton spatial wave function, developed the data processing algorithms, and performed the experiments of biphoton propagation dynamics and saddle phase modulation. This method requires only one measurement and is reference-free, but the spatial resolution is the major shortcoming. Amplitude and phase patterns with higher spatial complexities cannot be detected without magnification. Although the CPD width limit in the multiple frame method is greatly lowered with the microlens array, the signal-to-noise ratio still hinders the detection of far wider CPDs, which may be overcome by a time-stamping camera like Tpx3Cam [17,50]. Recently, another wavefront sensor based on spatial masking and diffraction with a high resolution was invented [52], which may be considered in quantum wavefront sensing in the future.

Classical SHWS has been widely used in fields like astronomy, laser optics, and biomedical imaging, while QSHWS can be applied in various tasks in the emerging field of adaptive quantum optics [42,43]. The phase information that lies in the second-order correlation can be assisted in astronomical observation, multiphoton physical optics [41], and free-space quantum communication against atmospheric turbulence. When studying multiphoton interaction or modulation media like nonlinear crystals and atom ensembles [53], the correlated phase aberration cannot be measured classically, while QSHWS may be the solution.

Theoretically, the single-pixel CPD shown in Fig. 2(a) provides more information of the biphoton field, linking the combination of the position and phase gradient of one photon to that of the other. For example, it reveals some properties of mixed states [44,45] and might be used for information encoding and secret sharing. Although the photon pairs are indistinguishable in our experiments, they can be spatially separated or have different wavelengths. This method is not limited to two photons [27]. If the JPD of more photons can be measured, the multiphoton wave function can also be reconstructed, leading to the measurement of higher-order correlations. Finally, this wavefront sensing technique can also be used in other continuous-variable degrees of freedom, such as frequency, by converting them into spatial entanglement [54,55], as well as combining topology and entanglement [56] in quantum optics.

This work was supported by the Innovation Program for Quantum Science and Technology (No. 2021ZD0301200 and No. 2021ZD0301400), National Natural Science Foundation of China (No. 62005263, No. 11821404, No. U19A2075, and No. 92365205), Anhui Initiative in Quantum Information Technologies (No. AHY060300), the Fundamental Research Funds for the Central Universities (No. WK2030000069), and the China Postdoctoral Science Foundation (No. 478 2020M671862).

Y. Z. and Z.-D. L. contributed equally to this letter.

*Contact author: zdliu@ustc.edu.cn
†Contact author: jsxu@ustc.edu.cn
‡Contact author: cfli@ustc.edu.cn

[1] F. Flamini, N. Spagnolo, and F. Sciarrino, Photonic quantum information processing: A review, Rep. Prog. Phys. **82**, 016001 (2018).
[2] O. S. Magaña-Loaiza and R. W. Boyd, Quantum imaging and information, Rep. Prog. Phys. **82**, 124401 (2019).
[3] T. B. Pittman, Y. H. Shih, D. V. Strekalov, and A. V. Sergienko, Optical imaging by means of two-photon quantum entanglement, Phys. Rev. A **52**, R3429 (1995).
[4] G. B. Lemos, V. Borish, G. D. Cole, S. Ramelow, R. Lapkiewicz, and A. Zeilinger, Quantum imaging with undetected photons, Nature (London) **512**, 409 (2014).
[5] H. Defienne, M. Reichert, J. W. Fleischer, and D. Faccio, Quantum image distillation, Sci. Adv. **5**, eaax0307 (2019).
[6] V. Giovannetti, S. Lloyd, L. Maccone, and J. H. Shapiro, Sub-Rayleigh-diffraction-bound quantum imaging, Phys. Rev. A **79**, 013827 (2009).
[7] Z. He, Y. Zhang, X. Tong, L. Li, and L. V. Wang, Quantum microscopy of cells at the Heisenberg limit, Nat. Commun. **14**, 2441 (2023).
[8] W.-W. Pan, X.-Y. Xu, Y. Kedem, Q.-Q. Wang, Z. Chen, M. Jan, K. Sun, J.-S. Xu, Y.-J. Han, C.-F. Li, and G.-C. Guo, Direct measurement of a nonlocal entangled quantum state, Phys. Rev. Lett. **123**, 150402 (2019).
[9] J. S. Lundeen, B. Sutherland, A. Patel, C. Stewart, and C. Bamber, Direct measurement of the quantum wavefunction, Nature (London) **474**, 188 (2011).
[10] J. C. Howell, R. S. Bennink, S. J. Bentley, and R. W. Boyd, Realization of the Einstein-Podolsky-Rosen paradox using momentum- and position-entangled photons from spontaneous parametric down conversion, Phys. Rev. Lett. **92**, 210403 (2004).
[11] J. Wang, J.-Y. Yang, I. M. Fazal, N. Ahmed, Y. Yan, H. Huang, Y. Ren, Y. Yue, S. Dolinar, M. Tur, and A. E. Willner, Terabit free-space data transmission employing orbital angular momentum multiplexing, Nat. Photonics **6**, 488 (2012).

[12] Y. Park, C. Depeursinge, and G. Popescu, Quantitative phase imaging in biomedicine, Nat. Photonics **12**, 578 (2018).

[13] D. Gabor, A new microscopic principle, Nature (London) **161**, 777 (1948).

[14] I. Yamaguchi and T. Zhang, Phase-shifting digital holography, Opt. Lett. **22**, 1268 (1997).

[15] H. Defienne, B. Ndagano, A. Lyons, and D. Faccio, Polarization entanglement-enabled quantum holography, Nat. Phys. **17**, 591 (2021).

[16] R. Camphausen, Álvaro Cuevas, L. Duempelmann, R. A. Terborg, E. Wajs, S. Tisa, A. Ruggeri, I. Cusini, F. Steinlechner, and V. Pruneri, A quantum-enhanced wide-field phase imager, Sci. Adv. **7**, eabj2155 (2021).

[17] D. Zia, N. Dehghan, A. D'Errico, F. Sciarrino, and E. Karimi, Interferometric imaging of amplitude and phase of spatial biphoton states, Nat. Photonics **17**, 1009 (2023).

[18] F. Zernike, How I discovered phase contrast, Science **121**, 345 (1955).

[19] J. Dressel, M. Malik, F. M. Miatto, A. N. Jordan, and R. W. Boyd, Colloquium: Understanding quantum weak values: Basics and applications, Rev. Mod. Phys. **86**, 307 (2014).

[20] Z. Shi, M. Mirhosseini, J. Margiewicz, M. Malik, F. Rivera, Z. Zhu, and R. W. Boyd, Scan-free direct measurement of an extremely high-dimensional photonic state, Optica **2**, 388 (2015).

[21] S. Kocsis, B. Braverman, S. Ravets, M. J. Stevens, R. P. Mirin, L. K. Shalm, and A. M. Steinberg, Observing the average trajectories of single photons in a two-slit interferometer, Science **332**, 1170 (2011).

[22] M. Yang, Y. Xiao, Y.-W. Liao, Z.-H. Liu, X.-Y. Xu, J.-S. Xu, C.-F. Li, and G.-C. Guo, Zonal reconstruction of photonic wavefunction via momentum weak measurement, Laser Photonics Rev. **14**, 1900251 (2020).

[23] R. H. Hudgin, Wave-front reconstruction for compensated imaging, J. Opt. Soc. Am. **67**, 375 (1977).

[24] W. Southwell, Wave-front estimation from wave-front slope measurements, J. Opt. Soc. Am. **70**, 998 (1980).

[25] Y. Zheng, M. Yang, Z.-H. Liu, J.-S. Xu, C.-F. Li, and G.-C. Guo, Detecting momentum weak value: Shack–Hartmann versus a weak measurement wavefront sensor, Opt. Lett. **46**, 5352 (2021).

[26] Y. Zheng, M. Yang, Z.-H. Liu, J.-S. Xu, C.-F. Li, and G.-C. Guo, Toward practical weak measurement wavefront sensing: Spatial resolution and achromatism, Opt. Lett. **47**, 2734 (2022).

[27] Y. Zheng, M. Yang, Y.-W. Liao, J.-S. Xu, C.-F. Li, and G.-C. Guo, Reconstructing the multiphoton spatial wave function with coincidence wave-front sensing, Phys. Rev. A **107**, 042608 (2023).

[28] X.-M. Hu, W.-B. Xing, B.-H. Liu, Y.-F. Huang, C.-F. Li, G.-C. Guo, P. Erker, and M. Huber, Efficient generation of high-dimensional entanglement through multipath down-conversion, Phys. Rev. Lett. **125**, 090503 (2020).

[29] B. C. Platt and R. Shack, History and principles of Shack-Hartmann wavefront sensing, J. Refract. Surg. **17**, S573 (2001).

[30] J. Ares, T. Mancebo, and S. Bará, Position and displacement sensing with Shack–Hartmann wave-front sensors, Appl. Opt. **39**, 1511 (2000).

[31] See Supplemental Material at http://link.aps.org/supplemental/10.1103/PhysRevLett.133.033602 for details of the experimental setup, data processing, more figures, and theoretical analyses.

[32] S. Walborn, C. Monken, S. Pádua, and P. Souto Ribeiro, Spatial correlations in parametric down-conversion, Phys. Rep. **495**, 87 (2010).

[33] J. Schneeloch and J. C. Howell, Introduction to the transverse spatial correlations in spontaneous parametric down-conversion through the biphoton birth zone, J. Opt. **18**, 053501 (2016).

[34] H. Defienne, M. Reichert, and J. W. Fleischer, General model of photon-pair detection with an image sensor, Phys. Rev. Lett. **120**, 203604 (2018).

[35] M. Reichert, H. Defienne, and J. W. Fleischer, Optimizing the signal-to-noise ratio of biphoton distribution measurements, Phys. Rev. A **98**, 013841 (2018).

[36] B. Ndagano, H. Defienne, D. Branford, Y. D. Shah, A. Lyons, N. Westerberg, E. M. Gauger, and D. Faccio, Quantum microscopy based on Hong–Ou–Mandel interference, Nat. Photonics **16**, 384 (2022).

[37] K. W. Chan, J. P. Torres, and J. H. Eberly, Transverse entanglement migration in Hilbert space, Phys. Rev. A **75**, 050101(R) (2007).

[38] A. Bhattacharjee, M. K. Joshi, S. Karan, J. Leach, and A. K. Jha, Propagation-induced revival of entanglement in the angle-OAM bases, Sci. Adv. **8**, eabn7876 (2022).

[39] C. K. Law and J. H. Eberly, Analysis and interpretation of high transverse entanglement in optical parametric down conversion, Phys. Rev. Lett. **92**, 127903 (2004).

[40] M. Reichert, X. Sun, and J. W. Fleischer, Quality of spatial entanglement propagation, Phys. Rev. A **95**, 063836 (2017).

[41] B. E. A. Saleh, M. C. Teich, and A. V. Sergienko, Wolf equations for two-photon light, Phys. Rev. Lett. **94**, 223601 (2005).

[42] H. Defienne, M. Reichert, and J. W. Fleischer, Adaptive quantum optics with spatially entangled photon pairs, Phys. Rev. Lett. **121**, 233601 (2018).

[43] P. Cameron, B. Courme, C. Vernière, R. Pandya, D. Faccio, and H. Defienne, Adaptive optical imaging with entangled photons, Science **383**, 1142 (2024).

[44] Z. Hradil, J. Řeháček, and L. L. Sánchez-Soto, Quantum reconstruction of the mutual coherence function, Phys. Rev. Lett. **105**, 010401 (2010).

[45] B. Stoklasa, L. Motka, J. Rehacek, Z. Hradil, and L. L. Sánchez-Soto, Wavefront sensing reveals optical coherence, Nat. Commun. **5**, 3275 (2014).

[46] Y. Zhou, J. Zhao, D. Hay, K. McGonagle, R. W. Boyd, and Z. Shi, Direct tomography of high-dimensional density matrices for general quantum states of photons, Phys. Rev. Lett. **127**, 040402 (2021).

[47] The symbol ∇_1 means taking the gradient with respect to the first vector variable. For example, $\nabla_1 f(\boldsymbol{\rho},\boldsymbol{\rho}) = \nabla_{\boldsymbol{\rho}'} f(\boldsymbol{\rho}',\boldsymbol{\rho})|_{\boldsymbol{\rho}'=\boldsymbol{\rho}}$.

[48] J. W. Goodman, *Introduction to Fourier Optics*, 4th ed. (W. H. Freeman, San Francisco, 2017).

[49] D. Eimerl, L. Davis, S. Velsko, E. K. Graham, and A. Zalkin, Optical, mechanical, and thermal properties of barium borate, J. Appl. Phys. **62**, 1968 (1987).

[50] B. Courme, C. Vernière, P. Svihra, S. Gigan, A. Nomerotski, and H. Defienne, Quantifying high-dimensional spatial entanglement with a single-photon-sensitive time-stamping camera, Opt. Lett. **48**, 3439 (2023).
[51] A. Einstein, B. Podolsky, and N. Rosen, Can quantum-mechanical description of physical reality be considered complete?, Phys. Rev. **47**, 777 (1935).
[52] S. Yi, J. Xiang, M. Zhou, Z. Wu, L. Yang, and Z. Yu, Angle-based wavefront sensing enabled by the near fields of flat optics, Nat. Commun. **12**, 6002 (2021).
[53] G. Nirala, S. T. Pradyumna, A. Kumar, and A. M. Marino, Information encoding in the spatial correlations of entangled twin beams, Sci. Adv. **9**, eadf9161 (2023).
[54] Z.-D. Liu, H. Lyyra, Y.-N. Sun, B.-H. Liu, C.-F. Li, G.-C. Guo, S. Maniscalco, and J. Piilo, Experimental implementation of fully controlled dephasing dynamics and synthetic spectral densities, Nat. Commun. **9**, 3453 (2018).
[55] Z.-D. Liu, Y.-N. Sun, B.-H. Liu, C.-F. Li, G.-C. Guo, S. Hamedani Raja, H. Lyyra, and J. Piilo, Experimental realization of high-fidelity teleportation via a non-Markovian open quantum system, Phys. Rev. A **102**, 062208 (2020).
[56] P. M. Tam, M. Claassen, and C. L. Kane, Topological multipartite entanglement in a Fermi liquid, Phys. Rev. X **12**, 031022 (2022).